

- [12] H. Kikuchi, M. Yokota, Y. Hisakado, H. Yang, T. Kajiyama, *Nat. Mater.* **2002**, *1*, 64.
- [13] Y. Hisakado, H. Kikuchi, T. Nagamura, T. Kajiyama, *Adv. Mater.* **2005**, *17*, 97.
- [14] M. J. Sansone, G. Khanarian, T. M. Leslie, M. Stiller, J. Altman, P. Elizondo, *J. Appl. Phys.* **1990**, *67*, 4253.
- [15] M. J. Sansone, G. Khanarian, M. S. Kwiatek, *J. Appl. Phys.* **1994**, *75*, 1715.
- [16] S. Matsumoto, M. Houlbert, T. Hayashi, K. Kubodera, *Appl. Phys. Lett.* **1996**, *69*, 1044.
- [17] S. Matsumoto, M. Houlbert, T. Hayashi, K. Kubodera, *Mater. Res. Soc. Symp. Proc.* **1997**, *457*, 89.
- [18] S. Matsumoto, Y. Sugiura, S. Sakata, T. Hayashi, *Liq. Cryst.* **2000**, *27*, 649.
- [19] J. J. Stankus, R. Torre, M. D. Fayer, *J. Phys. Chem.* **1993**, *97*, 9478.
- [20] S. D. Gottke, D. D. Brace, H. Cang, B. Bagchi, M. D. Fayer, *J. Chem. Phys.* **2002**, *116*, 360.
- [21] P. Kedziora, J. Jadzyn, L. Hellems, *Phys. Rev. B: Condens. Matter Mater. Phys.* **2002**, *66*, 031702.
- [22] The optical properties of the composites were dependent on the fraction of chiral dopant. The 11.5 wt.-% fraction reported here is for a composite that was amongst the best in terms of transparency and isotropy in our experiments. Detailed results of the dependence of the optical properties of the composites on the chiral dopant fraction will be reported elsewhere.
- [23] B. Chu, C. S. Bak, F. L. Lin, *Phys. Rev. Lett.* **1972**, *28*, 1111.

High-Performance Ambipolar Pentacene Organic Field-Effect Transistors on Poly(vinyl alcohol) Organic Gate Dielectric**

By Thokchom Birendra Singh,* Farideh Meghdadi, Serap Günes, Nenad Marjanovic, Gilles Horowitz, Philippe Lang, Siegfried Bauer, and Niyazi Serdar Sariciftci

Organic field-effect transistors (OFETs) based on small molecules, polymers, and composites are the subject of intensive research.^[1,2] Most of the reported transistors use organic

semiconductors capable of transporting either only holes (p-type)^[3-5] or only electrons (n-type),^[6,7] with the large majority being p-type, such as phthalocyanines, oligothiophenes, etc. The field-effect mobility is largely determined by the morphology of the semiconductor film at the interface with the gate dielectric.^[8] Early studies of interface-related effects were concerned with the chemical modification of the dielectric surface, for example, with self-assembled monolayers or by surface passivation of the commonly used SiO₂ or Al₂O₃ dielectrics, with the modified surfaces resulting in optimized interfaces and higher crystallinity for the semiconductor growth.^[9] Recently, organic gate dielectrics^[10-15] were introduced as an alternative to inorganic gate oxide-type dielectrics. Organic dielectrics i) can be solution processed, ii) provide smooth films on transparent glass and plastic substrates, iii) are suitable for optoelectronic applications like photo-responsive OFETs due to their high optical transparency, iv) can be thermally stable up to 200 °C with a relatively small thermal expansion coefficient, and v) can possess a rather high dielectric constant, on the order of 10. The performance of OFETs with organic gate dielectrics critically depends on the choice of the gate dielectric.^[16] The use of special gate electrets, for example, allows for the production of non-volatile, all-organic field-effect transistor memory elements.^[17-19]

In field-effect transistors with a hydroxy-group-free interface between the semiconductor and the polymeric gate dielectric, it has been observed that n-type carrier transport is feasible in most organic semiconductors.^[20] Two-dimensional numerical simulations on metal-insulator-semiconductor structure devices suggested that electron transport in p-type organic semiconductors is possible with sufficiently small channel lengths and ohmic source-drain electrodes.^[21] Ambipolar charge transport, the simultaneous or selective transport of electrons and holes in OFETs, is of interest from a fundamental scientific as well as from an application point of view.^[22-31] In organic electronics, so far very little is known about the correlation of ambipolar transport^[32] with the morphology of organic semiconducting thin films at the interface between the organic semiconductor and the gate dielectric.^[33] Electron transport properties are more sensitive to the purity of the crystal.^[32]

The current benchmark material for high-performance OFETs is vacuum-evaporated pentacene.^[34] Conducting probe atomic force microscopy measurements on single pentacene islands have shown that pentacene can conduct both electrons and holes (i.e., is ambipolar).^[35] Here we have chosen pentacene and *para*-hexaphenyl (PHP) in order to investigate ambipolar charge transport in these semiconductors. As gate dielectrics, poly(4-vinyl phenol) (PVP) and poly(vinyl alcohol) (PVA) polymers are employed. PVP and PVA differ by their surface energy (35 and 45 mJ m⁻², respectively) and dielectric constant (3.9 and 8, respectively). It seems that growing the organic semiconducting film on gate dielectrics with a different surface energy and dielectric constant results in a change of the morphology of the semiconductor film. Ambipolar charge transport is observed in PVA dielectric

[*] Dr. Th. B. Singh, Dr. F. Meghdadi, S. Günes, N. Marjanovic, Prof. N. S. Sariciftci
Linz Institute of Organic Solar Cells (LIOS)
Physical Chemistry, Johannes Kepler University Linz
A-4040 Linz (Austria)
E-mail: birendra.singh@jku.at

Dr. G. Horowitz, Dr. P. Lang
ITODYS, CNRS-UMR 7086
University Denis-Diderot
1 rue Guy de la Brosse, F-75005 Paris (France)

Prof. S. Bauer
Soft Matter Physics (SOMAP)
Johannes Kepler University Linz
A-4040 Linz (Austria)

[**] Th.B.S. acknowledges the financial support of the Austrian Foundation for the Advancement of Science (FWF NANORAC contract No. N00103000).

FET devices. The observation is supported by quasi-static capacitance–voltage measurements on metal–insulator–semiconductor structure devices.

The two chosen organic semiconductors pentacene^[34] and PHP^[36] as well as the two organic dielectrics PVP^[10,15] and PVA,^[14,16] have previously been well studied. The water content of the two polymers is difficult to estimate, though it is expected to have an influence on the dielectric constant and charging dynamics. A simplified energy band diagram of pentacene^[37] with Au electrodes in the absence of a bias potential and of interface dipoles is depicted in Figure 1a. Note that these are actual barrier heights as estimated from the ultraviolet photoelectron spectroscopy (UPS) and reverse UPS mea-

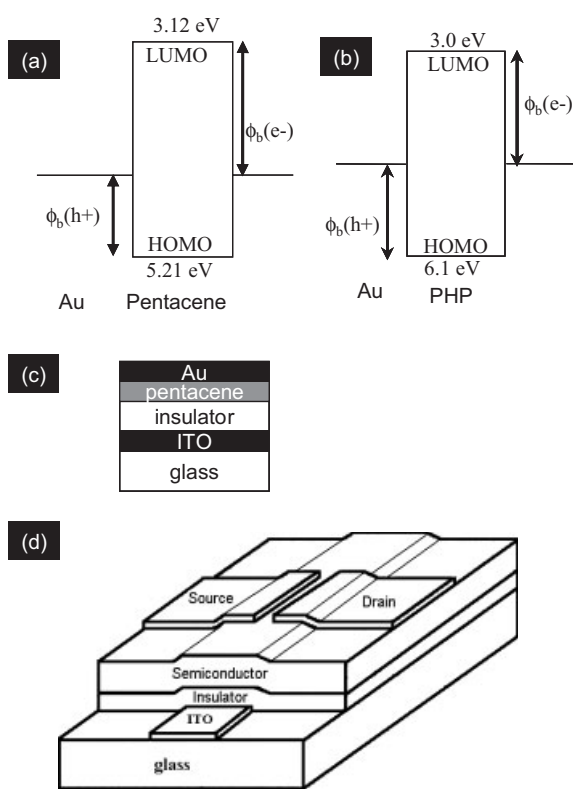


Figure 1. a) Simplified energy band diagram of pentacene with Au. b) PHP with Au (from [37]). Schematic diagram of the device structure; c) metal–insulator–semiconductor (MIS) arrangement and d) top-contact pentacene OFET.

surements.^[37] Although one would expect the injection of electrons from gold into the lowest unoccupied molecular orbital (LUMO) of pentacene to be a difficult process due to the large injection barrier [$\phi_b(e^-) \sim 1.35$ eV, $\phi_b(h^+) \sim 0.85$ eV],^[37] we have achieved n-type FET operation by optimizing the pentacene film morphology at the interface with the organic dielectric. PVA has a higher surface energy and dielectric constant in comparison to PVP. This results in a stronger interaction between the dielectric surface and the pentacene molecules during evaporation, as evident from the

film morphology (see Fig. 2). Figures 2c,d depict small pentacene crystallites on PVA, while larger crystallites are obtained on PVP (Figs. 2a,b). In PVP, with the lower surface energy and lower dielectric constant, three-dimensional growth of pentacene is favored.^[10] Accordingly, transport properties are

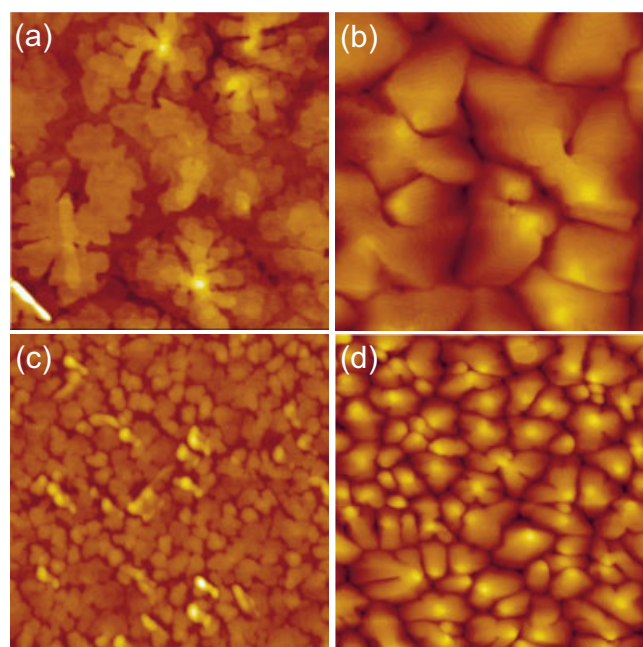


Figure 2. AFM topographical images ($2.5 \mu\text{m} \times 2.5 \mu\text{m}$) of room temperature grown a) 5 nm pentacene film on PVP, b) 50 nm pentacene film on PVP, c) 5 nm pentacene film on PVA, and d) 50 nm pentacene film on PVA.

found to be very different for the two cases studied, probably because of the different film morphology. In the field-effect transistor experiment, changes in the conductance along the semiconductor surface is studied as a function of an electric field applied normal to the surface. An alternative method for charge injection studies is provided by capacitance–voltage measurements on metal–insulator–semiconductor (MIS) structures.

The quasi-static capacitance, C , of the MIS structure versus gate voltage, V_{gs} , is shown in Figure 3 for pentacene grown on PVP (Fig. 3a) and PVA (Fig. 3b). Over one hundred different devices were measured and showed a deviation of about 20% in the total capacitance. In the MIS structure, the capacitance is modelled as a serial connection of the gate dielectric capacitance and the capacitance of the semiconducting layer. The measured capacitance approaches the capacitance of the pure dielectric (1.2 and 1.8 nF cm⁻² for PVP and PVA, respectively), whenever charges are attracted to the interface between the semiconductor and the dielectric, e.g., for hole and electron accumulation, respectively. As shown in Figure 3a, in the case of PVP, we have only observed hole accumulation, as evident from the increase of the capacitance at negative V_{gs} .

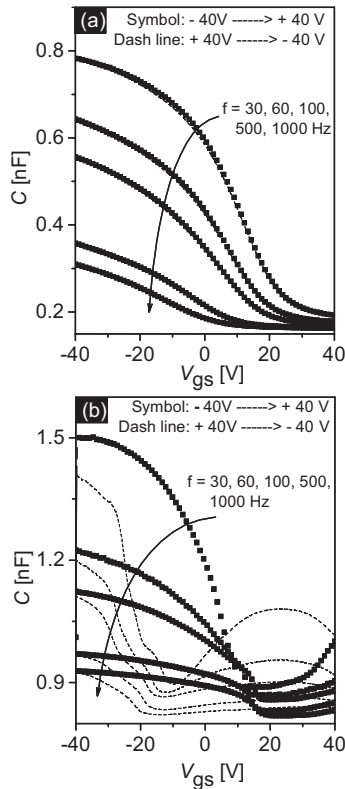


Figure 3. Room temperature quasi-static capacitance–voltage curves for the MIS structures in Fig. 1b with a) PVP (applied alternating current (ac) voltage of 1 V at different frequencies with a scan rate of 0.02 V s^{-1}) and b) PVA as a dielectric. For PVA, the accumulation of both electrons and holes at the interface seems possible, whereas for PVP, only the accumulation of holes is found.

Electron accumulation is not observed, since the capacitance of the MIS structure decreases with increasing V_{gs} . The results suggest an increasing depletion region with increasing V_{gs} and no electron accumulation at the interface. Note that the C – V_{gs} curves are practically the same in sweeps with increasing and decreasing gate bias voltage levels with no apparent hysteresis. In Figure 3b, for the PVA dielectric, a completely different behavior of the capacitance versus V_{gs} is seen. On the left side, with negative V_{gs} , we have also observed hole accumulation, as in the case of PVP. However, on the right side, at positive V_{gs} , we have found an increasing capacitance with increasing gate voltage. This result may be interpreted in terms of electron accumulation, though the large hysteresis obtained on sweeping the gate voltage from negative to positive bias and vice versa is puzzling. In conventional inorganic MIS, the frequency dependence (that is, the decrease of the capacitance in the accumulation or inversion regime) is attributed to interface states. Further work is needed to extend such an explanation to organic structures.

The C – V_{gs} measurements clearly revealed single carrier transport in pentacene on PVP and a possibility for ambipolar transport in pentacene on PVA. Therefore, we have studied the features of pentacene OFET structures (Fig. 1c) with PVP

and PVA dielectrics, respectively. According to the above discussion, pentacene films grown on PVP are expected to give rise to an OFET with hole-only accumulation, whereas pentacene films on PVA may accumulate both electrons or holes at the interface depending on the bias applied. Figure 4a shows the output characteristics of pentacene OFETs with Au as the source–drain electrode using PVP as a dielectric to demonstrate only the transport of holes (dominantly single carrier

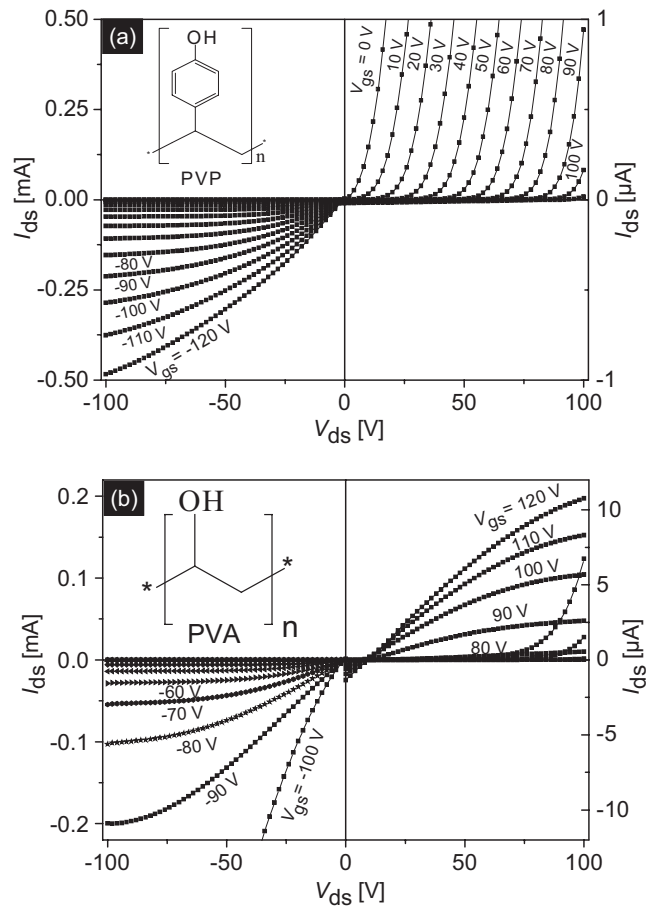


Figure 4. a) Output characteristics of a single-carrier-type pentacene OFET on PVP. b) Ambipolar pentacene OFET on PVA. All measurements are performed with steps of 2 V s^{-1} . The insets show the chemical structure of PVP and PVA, respectively. Note: the left and right scales correspond to the p-channel and n-channel mode characteristics, respectively.

type), as expected from the C – V_{gs} measurements shown in Figure 3a. Ambipolar transport is observed in pentacene OFETs with Au source–drain electrodes on the PVA dielectric (Fig. 4b). The threshold voltage, V_t , is found to be different for OFETs with PVP and PVA as gate dielectrics, although the thickness of the dielectrics is essentially the same. In the case of PVA, one would expect the injection of electrons from gold into pentacene to be a difficult process (see Fig. 1a) because of the mismatch in the energies of the LUMO level of pentacene and the workfunction of gold

$[\varphi_b(e^-) = 1.3 \text{ eV}]$. However, in spite of this, the transistor works at a relatively low threshold voltage, a V_t of 18 V (in n-channel mode), with a drain current of $I_{ds} \approx 10^{-5} \text{ A}$ for an applied gate bias of $V_{gs} = +120 \text{ V}$. The transistor characteristics were also measured by using Ca/Al as a source–drain electrode, where transistors lose their meaning in the case of PVP and ambipolar transport in the case of PVA. The n-channel mode in the case of PVP shows a $I_{ds}(V_{ds})$ similar to a diode characteristic, which is in agreement with the capacitance–voltage measurements indicating a reverse biased p–n junction (Fig. 3b). In the case of PVA, I_{ds} is the sum of both hole and electron currents at lower V_{gs} (Fig. 4b) and above the V_t , I_{ds} seems to be predominantly a result of the accumulation of electrons at the interface of the semiconductor and insulator, which is a unique feature of ambipolar transport. The V_t for such a selective transport is also seen in the transfer characteristics presented in Figure 5.

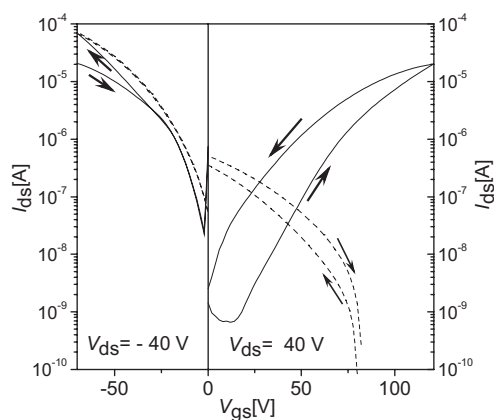


Figure 5. Transfer characteristics of pentacene OFETs using PVP (dashed line) and PVA (solid line). All measurements are done with steps of 2 V s^{-1} . Ambipolar transport is observed in OFETs on PVA with a small hysteresis. Mobilities obtained from the curves are summarized in Table 1.

Figure 5 shows the comparison of the transfer characteristics of the two pentacene OFETs, which demonstrate strikingly different transport properties. Devices on PVP with a p-channel mode show the largest on current, which is analogous to the output characteristics previously shown in Figure 4a. In the n-channel mode, the hole current is further

depleted by applying a larger V_{gs} and there is no evidence for an electron current. For the devices on PVA, both p-channel and n-channel formation is observed, which is analogous to the output characteristics shown previously (Fig. 4c). When the direction of V_{gs} is reversed we generally observed a sizeable hysteresis. The hysteresis observed in PVA-based devices is quite well known, and is attributed to the presence of mobile ionic charges.^[16]

The drain current depends quadratically on the applied V_{gs} . This allows estimation of the mobility, μ from:^[38]

$$I_{ds} = \frac{\mu W C_i}{2L} (V_{gs} - V_t)^2 \quad (1)$$

where W is the channel width, L is the channel length, and C_i is the dielectric capacitance. In the estimation of the field-effect mobility, a V_{gs} independent mobility is assumed and for simplicity contact resistances were not taken into account. The field-effect mobilities obtained from the forward curves are summarized in Table 1. Mobilities obtained from devices where the semiconducting film was grown at an elevated temperature of 50°C are comparatively higher, as reported in the literature.^[39]

Additional experiments that involved growing a PHP film on PVA resulted in OFETs (with Au as a source–drain electrode) with ambipolar output characteristics. As shown in Figure 1b, the electron-injection barrier, $\varphi_b(e^-)$ from the Au electrode to the LUMO level of PHP is 1.3 eV and the hole-injection barrier, $\varphi_b(h^+)$ from the Au electrode to the highest occupied molecular orbital (HOMO) level of PHP is 1.8 eV.^[37] These energy barriers are comparable with pentacene. Due to this high barrier, the current is mainly limited by injection. The contact resistance in ambipolar OFETs^[29,30] is strongly reduced with increasing V_{gs} , which can be interpreted in terms of tunnel injection through a thin barrier.^[40,41] Our finding is that organic semiconductors can be ambipolar on hydroxy-terminated dielectrics. This may be seen as an interesting result since it has been suggested in the literature^[20] that surface dipoles make n-channel behavior less likely.

Although ambipolar transistors cannot, as such, be used to realize complementary circuits, they have great potential for complementary-like circuits.^[26,30] Our results reveal evidence for a possibility of n-type behavior in pentacene-based OFETs, which in conjunction with a p-type operating mode would allow the completion of such circuits.

Table 1. Summary of parameters extracted from the OFETs fabricated using PVP and PVA gate dielectrics. The values shown here are an average of at least ten different devices fabricated under identical conditions.

Dielectric	Semiconductor	Dispersive surface energy [a] [mJ m ⁻²]	Threshold voltage (V_t) (hole, electron) [V]	Hole mobility (μ_h) [cm ² V ⁻¹ s ⁻¹]	Electron mobility (μ_e) [cm ² V ⁻¹ s ⁻¹]
PVP	pentacene (RT)	35	0	0.5	Not active
PVA	pentacene (RT)	45	-10.18	0.4	0.05
	pentacene (50 °C)	–	-27.57	0.5	0.2
PVA	para-hexaphenyl (RT)	–	-30.80	0.02	0.001

[a] The constant contact angles obtained for PVP and PVA on dielectric films thicker than $1 \mu\text{m}$ are used to evaluate the interfacial dispersive surface energies. The surface energy reported here is comparable with one reported in the literature [42].

In conclusion, we have shown ambipolar transport in OFETs grown on PVA as a gate dielectric. PVA affects the growth of the semiconductor, where smaller grain sizes accompany the ambipolar charge transport properties with a high electron mobility of $0.05 \text{ cm}^2 \text{ V}^{-1} \text{ s}^{-1}$ and a hole mobility of $0.4 \text{ cm}^2 \text{ V}^{-1} \text{ s}^{-1}$ using contacts such as gold. The present study indicates that the morphology of the semiconductor interface at the organic semiconductor/organic dielectric is a critical parameter for OFET properties such as ambipolar transport. A correlation of thin-film nanomorphology and ambipolar transport is established for normally unipolar high-mobility organic materials.

Experimental

Indium titanium oxide (ITO) glasses were cut to $15 \text{ mm} \times 15 \text{ mm}$ in size and were etched to leave an area of $0.5 \text{ mm} \times 15 \text{ mm}$ as a gate electrode. After cleaning the glass with acetone and propan-2-ol in an ultrasonic bath, the polymer dielectric was spun from solution onto its surface. The area of the gate dielectric was optimized by removal of the thin film with the respective solvent. Poly(vinyl alcohol) (PVA) (Mowiol®40–88) with an average molecular weight of 120 000 (Sigma–Aldrich) and poly(4-vinyl phenol) (PVP) with average molecular weight of 50 000 (Sigma–Aldrich) were used as received. All the dielectrics, PVP (10 % in propan-2-ol) and PVA (10 % in water), were spun at 1500 rpm on top of the ITO glasses. To ensure that all the solvent was removed from the PVA and PVP film, the films were dried in an Ar atmosphere at 60°C and left overnight. The average thicknesses of the two dielectrics are about $1\text{--}1.5 \text{ }\mu\text{m}$. Pentacene and *para*-hexylphenyl were used as received from Sigma–Aldrich. Organic thin-films were grown at the rate of $0.2\text{--}0.3 \text{ \AA s}^{-1}$ at room temperature at a base vacuum of 10^{-6} mbar. We used Leybold Univex 350 which has a source-to-substrate height of about 0.5 m . Subsequent metal evaporations were performed under a vacuum of 9×10^{-7} mbar using a shadow mask. Separate MIS structure devices with Au (60 nm) as top electrodes were prepared for the quasi-static capacitance–voltage measurements. Device transportation from the evaporation chamber to the glove box for metal evaporation and all further electrical characterization was carried out under an argon environment. Other metals, such as Ca/Al and Mg/Al, were also evaporated for comparative studies. The channel length, L , of the device is $20\text{--}25 \text{ }\mu\text{m}$ and the channel width is $W=1\text{--}1.5 \text{ mm}$, giving a W/L ratio of $50\text{--}100$. An Agilent E5273A with two source-measure unit instrument was employed for the steady state current–voltage measurements. In addition, Keithley 2400 and 236 source-measure unit instruments were also employed to reconfirm all the electrical measurements. All measurements were performed with a scan rate of 2 V s^{-1} unless otherwise stated. For quasi-static capacitance–voltage measurements, we used a HP 4248A precision LCR meter with a typical scan rate of 0.02 V s^{-1} . The surface morphology and the thickness of the dielectric and organic thin-films were measured under ambient conditions with a Digital Instrument Dimension 3100 atomic force microscope. A comparison of the measured dielectric capacitances under inert conditions with the thickness of the dielectric layer consistently gave values of the dielectric constant, ϵ , of 3.9 and 8, and capacitance, C_i , of 1.2 and 1.8 nF cm^{-2} for PVP and PVA, respectively, which was in agreement with the previously published values [16].

Received: May 30, 2005

Final version: June 24, 2005

Published online: August 16, 2005

- [1] C. D. Dimitrakopoulos, P. R. L. Malenfant, *Adv. Mater.* **2002**, *14*, 99.
[2] G. Horowitz, *J. Mater. Res.* **2004**, *19*, 1946.

- [3] H. Sirringhaus, N. Tessler, R. H. Friend, *Science* **1998**, *280*, 1741.
[4] C. D. Dimitrakopoulos, S. Purushothaman, J. Kymissis, A. Callegari, J. M. Shaw, *Science* **1999**, *283*, 822.
[5] R. C. Haddon, A. S. Perel, R. C. Morris, T. T. M. Palstra, A. F. Hebard, R. M. Fleming, *Appl. Phys. Lett.* **1995**, *67*, 121.
[6] J. G. Laquindanum, H. E. Katz, A. Dodabalapur, A. J. Lovinger, *J. Am. Chem. Soc.* **1996**, *118*, 11 331.
[7] H. E. Katz, A. J. Lovinger, J. Johnson, C. Kloc, T. Siegrist, W. Li, Y.-Y. Lin, A. Dodabalapur, *Nature* **2000**, *404*, 478.
[8] F. Dinelli, M. Murgia, P. Levy, M. Cavallini, F. Biscarini, D. M. de Leeuw, *Phys. Rev. Lett.* **2004**, *92*, 116 802.
[9] a) W. Kalb, Ph. Lang, M. Mottaghi, H. Aubin, G. Horowitz, M. Wutting, *Synth. Met.* **2004**, *146*, 279. b) S. C. Lim, S. H. Kim, J. H. Lee, M. K. Kim, D. J. Kim, T. Zyung, *Synth. Met.* **2004**, *148*, 75. c) K. Sankar, T. N. Jackson, *J. Mater. Res.* **2004**, *19*, 2003. d) T. W. Kelly, L. D. Boardman, T. D. Dunbar, D. V. Muires, M. J. Pellerite, T. P. Smith, *J. Phys. Chem. B* **2003**, *107*, 5877.
[10] H. Klauk, M. Halik, U. Zschieschang, G. Schmid, W. Radlik, *J. Appl. Phys.* **2002**, *92*, 5259.
[11] J. Veres, S. D. Ogier, S. W. Leeming, D. C. Cupertino, S. M. Khaffaf, *Adv. Mater.* **2003**, *13*, 199.
[12] R. Parashkov, E. Becker, G. Ginev, T. Riedl, H. H. Johannes, W. Kowalsky, *J. Appl. Phys.* **2004**, *95*, 1594.
[13] J. Park, S. Y. Park, S. Shim, H. Kang, H. H. Lee, *Appl. Phys. Lett.* **2004**, *85*, 3283.
[14] R. Schroeder, L. A. Majewski, M. Grell, *Appl. Phys. Lett.* **2003**, *83*, 3201.
[15] D. Knipp, R. A. Street, B. Krusor, J. Ho, R. B. Apte, *Mater. Res. Soc. Symp. Proc.* **2002**, *708*, BB.10.
[16] Th. B. Singh, N. Marjanovic, P. Stadler, M. Auinger, G. J. Matt, S. Günes, N. S. Sariciftci, R. Schwödiauer, S. Bauer, *J. Appl. Phys.* **2005**, *97*, 083 714.
[17] R. Schroeder, L. A. Majewski, M. Grell, *Adv. Mater.* **2004**, *16*, 633.
[18] Th. B. Singh, N. Marjanovic, G. J. Matt, N. S. Sariciftci, R. Schwödiauer, S. Bauer, *Appl. Phys. Lett.* **2004**, *85*, 5409.
[19] R. C. G. Naber, C. Tanase, P. W. M. Blom, G. H. Gelinck, A. W. Marsman, F. J. Touwslager, S. Setayesh, D. M. De Leeuw, *Nat. Mater.* **2005**, *4*, 243.
[20] L. L. Chua, J. Zaumseil, J. Chang, E. C. W. Ou, P. K. H. Ho, H. Sirringhaus, R. H. Friend, *Nature* **2005**, *434*, 194.
[21] S. Scheinert, G. Paaasch, S. Pohlmann, H. H. Horhold, R. Stockmann, *Solid State Electron.* **2000**, *44*, 845.
[22] A. Dodabalapur, H. E. Katz, L. Torsi, R. C. Haddon, *Science* **1995**, *296*, 1560.
[23] A. Dodabalapur, H. E. Katz, L. Torsi, R. C. Haddon, *Appl. Phys. Lett.* **1996**, *68*, 1108.
[24] K. Tada, H. Harada, K. Yoshino, *Jpn. J. Appl. Phys., Part 2* **1996**, *35*, L944.
[25] a) R. Martel, V. Derycke, C. Lavoie, J. Appenzeller, K. K. Chan, J. Tersoff, Ph. Avouris, *Phys. Rev. Lett.* **2001**, *87*, 256 805. b) J. A. Misewich, R. Martel, Ph. Avouris, J. C. Tsang, S. Heinze, J. Tersoff, *Science* **2003**, *300*, 783.
[26] E. J. Meijer, D. M. de Leeuw, S. Setayesh, E. Van Veenendaal, B.-H. Huisman, P. W. M. Blom, J. C. Hummelen, U. Scherf, T. M. Klappwijk, *Nat. Mater.* **2003**, *2*, 678.
[27] R. J. Chesterfield, C. R. Newman, T. M. Pappenfus, P. C. Ewbank, M. H. Haukaas, K. R. Mann, L. L. Miller, C. D. Frisbie, *Adv. Mater.* **2003**, *15*, 1278.
[28] A. Babel, J. D. Wind, S. A. Jenekhe, *Adv. Func. Mater.* **2004**, *14*, 891.
[29] T. D. Anthopoulos, C. Tanase, S. Setayesh, E. J. Meijer, J. C. Hummelen, P. W. M. Blom, D. M. de Leeuw, *Adv. Mater.* **2004**, *16*, 2174.
[30] T. D. Anthopoulos, D. M. de Leeuw, E. Cantatore, S. Setayesh, E. J. Meijer, C. Tanase, J. C. Hummelen, P. W. M. Blom, *Appl. Phys. Lett.* **2004**, *85*, 4205.
[31] M. Ahles, R. Schmechel, H. V. Seggern, *Appl. Phys. Lett.* **2004**, *85*, 4499.

- [32] R. G. Keppler, *Phys. Rev.* **1960**, *119*, 1266.
 [33] Th. B. Singh, S. Günes, N. Marjanovic, R. Menon, N. S. Sariciftci, *J. Appl. Phys.* **2005**, *97*, 114 508.
 [34] Y. Y. Lin, D. J. Gundlack, S. F. Nelson, T. N. Jackson, *IEEE Electron. Device Lett.* **1997**, *18*, 606.
 [35] T. Heim, K. Lmimouni, D. Vuillaume, *Nano Lett.* **2004**, *4*, 2145.
 [36] D. J. Gundlack, Y. Y. Lin, T. N. Jackson, D. G. Schlom, *Appl. Phys. Lett.* **1997**, *71*, 3853.
 [37] N. Koch, A. Kahn, J. Ghijsen, J.-J. Pireaux, J. Schwartz, R. L. Johnson, A. Elschner *Appl. Phys. Lett.* **2003**, *82*, 70.
 [38] S. M. Sze, *Physics of Semiconductor Devices*, Wiley, New York **1981**.
 [39] M. Shtein, J. Mapel, J. B. Benziger, S. R. Forrest, *Appl. Phys. Lett.* **2002**, *81*, 268.
 [40] P. V. Pesavento, R. J. Chesterfield, C. R. Newman, C. D. Frisbie, *J. Appl. Phys.* **2004**, *96*, 7312.
 [41] L. Burgi, T. J. Richards, R. H. Friend, H. Sirringhaus, *J. Appl. Phys.* **2003**, *94*, 6129.
 [42] W. A. Zisman, in *Contact Angle, Wettability and Adhesion* (Ed: F. W. Fowkes), Advances in Chemistry Vol. 43, American Chemical Society, Washington, DC **1964**, p. 1.

One-Dimensional Quantum-Confinement Effect in α -Fe₂O₃ Ultrafine Nanorod Arrays**

By *Lionel Vayssieres**, *Conny Sathe*, *Sergei M. Butorin*, *David K. Shuh*, *Joseph Nordgren*, and *Jinghua Guo**

Bandgap and band-edge positions, as well as the overall band structure of semiconductors, are of crucial importance in photoelectrochemical and photocatalytic applications. The energy position of the band-edge level can be controlled by the electronegativity of the dopants, solution pH (flat band poten-

tial variation of 60 mV per pH unit), and by quantum confinement effects. Accordingly, band edges and the bandgap can be tailored to achieve specific electronic, optical, or photocatalytic properties. A very important application is found in the generation of H₂ from direct photo-oxidation of water without external bias.^[1] Indeed, to succeed in splitting water via solar irradiation, the valence band of the semiconductor has to be located at a lower energy level than the chemical potential of dioxygen evolution (H₂O/O₂), and the conduction band has to be located at a higher energy level than the chemical potential of dihydrogen evolution (H₂/H⁺). If the positions of the energy levels of the valence and conduction band are not fulfilled, an external bias has to be applied to induce the photocatalytic process, which in turn substantially reduces the overall efficiency. It has been reported that an optimal bandgap of 2.46 eV^[2] is required for water photo-oxidation without an external bias. Although the bandgap of hematite, reported to be around 1.9 to 2.2 eV (depending on its crystalline status and methods of preparation), and its valence band edge are suitable for oxygen evolution, the conduction band edge of hematite is too low to generate hydrogen. Therefore, a blue-shift of the bandgap of hematite of about 0.3 to 0.6 eV and the concomitant upward shift of the conduction band edge would make hematite an ideal anode material for photocatalytic devices for the photo-oxidation of water in terms of cost, abundance, and non-toxicity, as well as thermal and structural stability and photocorrosion resistance. Efficient photovoltaic properties have been demonstrated by the design of thin films of hematite consisting of crystalline arrays of oriented nanorods.^[3] They exhibited substantial photocurrent efficiencies due to better transport and collection of photogenerated electrons through a designed path (i.e., the oriented rods), as well as to a better physical and structural match between the n-type semiconductor material, the diameter of its nanometer-scale building blocks, and the minority carrier (hole) diffusion length.^[4] In the present report, we investigate quantum-confinement effects on bandgap profiling in similar arrays by resonant inelastic X-ray scattering for potential application of such nanomaterials in direct photo-oxidation of water by solar irradiation.

The formation of bundles of ultrafine hematite nanorods is understood by considering the crystal structure of β -FeOOH, which occurs in nature as the mineral akaganeite. It crystallizes in the tetragonal system (space group $I4/m (C_{4h}^5)$, $a = 10.44$, $c = 3.01$ Å). Its structure can be described as a tunnel structure (similar to α -MnO₂) hosting H₂O or Cl⁻ and is based on a defected close-packed oxygen lattice with three different kinds of oxygen layers (Fig. 1, bottom). Every third layer is only two-thirds occupied, with rows of oxygen atoms missing along the c -axis. The cation occupation of octahedral sites between the other anion layers is in double rows, but separated by single rows of empty sites along the c -axis. The octahedral cation sites remaining between the third anion layer and its neighbor layer are completely filled. This topology produces dioctahedral chains, which are arranged around the four-fold symmetric c -axis. The chains share vertices along their edges,

[*] Dr. L. Vayssieres
 ICYS, National Institute for Materials Science
 Namiki 1-1, Tsukuba 305-0044 (Japan)
 E-mail: vayssieres.lionel@nims.go.jp

Dr. J. Guo
 Advanced Light Source, Lawrence Berkeley National Laboratory
 Berkeley, CA 94720 (USA)
 E-mail: JGuo@lbl.gov

Dr. C. Sathe, Dr. S. M. Butorin, Prof. J. Nordgren
 Department of Physics, Uppsala University
 Box 530, SE-751 21 Uppsala (Sweden)

Dr. D. K. Shuh
 Chemical Sciences Division, Lawrence Berkeley National Laboratory
 Berkeley, CA 94720 (USA)

[**] The project was supported by the Swedish Natural Science Research Council (NFR), the Swedish Research Council for Engineering Sciences (TFR), and the Göran Gustafsson Foundation for Research in Natural Sciences and Medicine, and by special coordination funds for promoting Science and Technology from the Ministry of Education, Culture, Sports, Science and Technology of Japan. The work at the ALS and LBNL was supported by the Director, Office of Basic Energy Sciences, Division of Materials and Division of Chemical Sciences, Geosciences, and Biosciences of the U.S. Department of Energy at Lawrence Berkeley National Laboratory under contract No. DE-AC02-05CH11231.